https://doi.org/10.5194/essd-2024-54
Preprint. Discussion started: 21 March 2024

First comprehensive stable isotope dataset of diverse water units in a permafrost-dominated catchment on the Qinghai–Xizang Plateau

Yuzhong Yang[1, 2], Qingbai Wu[1, 2], Xiaoyan Guo[3], Lu Zhou[1], Helin Yao[1], Dandan[4] Zhang, Zhongqiong Zhang[1, 2], Ji Chen[1, 2], Guojun Liu[1, 2]

[1] State Key Laboratory of Frozen Soil Engineering, Northwest Institute of Eco-Environment and Resources, Chinese Academy of Sciences, Lanzhou, China

[2] Qinghai-Beiluhe Plateau Frozen Soil Engineering Safety National Observation and Research Station, China

[3] Key Laboratory of Ecohydrology of Inland River Basin, Northwest Institute of Eco-Environment and Resources, Chinese Academy of Sciences, Lanzhou, China

[4] College of Energy and Power Engineering, Lanzhou University of technology, Lanzhou, China

Correspondence to: Yuzhong Yang (yangyuzhong08@lzb.ac.cn)

https://doi.org/10.5194/essd-2024-54
Preprint. Discussion started: 21 March 2024

Open Access Earth System Science Data Discussions

Abstract

Considered as the Asian water tower, the Qinghai–Xizang Plateau (QXP) processes substantial permafrost, where its hydrological environments are spatially differed and can be easily disturbed by changing permafrost and melting ground ice. Permafrost degradation compels melting permafrost to become an important source of surface runoff, changes the storage of groundwater, and greatly influences the hydrological processes in permafrost regions. However, the evidences linking permafrost degradation and hydrological processes on the QXP are lacking, which increase the uncertainties of the evaluation results of changing permafrost on the water resources. Stable isotopes offer valuable information on the connections between changing permafrost (ground ice) and water components. It is therefore particularly important to observe the changes in the stable isotopes of different waterbodies, which can vary over hourly to annual timescales and truly capture the thawing signals and reflect the influence of permafrost (ground ice) on the regional hydrological processes. The Beiluhe Basin (BLH) in the hinterland of QXP were selected, which well integrates all the water components related to hydrological cycles, and is an ideal site to study hydrological effect of permafrost change. This paper presents the temporal data of stable isotopes ($\delta^{18}O$, δD, and d-excess) in different water bodies (precipitation, stream water, thermokarst lake, and groundwater) in the BLH produced between 2017 and 2022. In special, the first detailed stable isotope data of ground ice at 17 boreholes and 2 thaw slumps are presented. A detailed description of the sampling processes, sample pretreating processes, and isotopic data quality control is given. The data firstly described the full seasonal isotope amplitude in the precipitation, stream, and thermokarst lakes, and delineated the depth isotopic variability in ground ice. Totally, 554 precipitation samples, 2402 lakes/ponds samples, 675 stream water samples, 102 supra-permafrost water samples, and 19 sub-permafrost water samples were collected during six years' continuous sampling work. Importantly, 359 ground ice samples at different depths from 17 boreholes and 2 profiles were collected. This first data set provides a new basis for understanding the hydrological effects of permafrost degradation on the QXP. It also provides supports on the cryospheric study on the Northern Hemisphere.

1 Introduction

Recognized as the main components of cryosphere, permafrost plays critical roles in climate change, evolution of ecosystem, water cycle, and human activities (Brown et al., 1997). Throughout the past several decades, the thermal stability of permafrost has suffered serious threats (Cheng et al., 2019; Douglas et al., 2021; Biskaborn et al., 2019) caused by continuous global warming (IPCC, 2019). Latest IPCC report indicates that up to 24-69% of permafrost will disappear by 2100 (IPCC, 2019). Warming and thawing of permafrost and an overall reduction in the ice content have been predicted under future climate change scenarios (IPCC, 2019). Dramatic permafrost degradation and ground ice melting has changed the regional hydrological processes (Yang et al., 2011; Quinton and Baltzer, 2013; Rogger et al., 2017), enhanced the hydraulic connections (Connon et al., 2014; Cheng and Jin, 2013; Zhang et al., 2013), and compel ground ice to become an important source of surface runoff and lakes (Yang et al., 2019; Zhang et al., 2005; Lawrence and Slater, 2005). Accordingly, clarifying the influence of degrading permafrost on the ecohydrology and water resources is of great significance to the protection of eco-environment and effective utilization of fresh water in permafrost regions in the world.

The Qinghai–Xizang Plateau (QXP) is known as the "Asia Water Tower", which is considered as the headwater regions of many large rivers in Asia (Immerzeel et al., 2010). As the world's largest high-altitude permafrost regions (Cheng et al., 2019), the QXP contains as many as 1.06×10^6 km^2 of permafrost and 12700 km^3 of ground ice (Cheng et al., 2019). Extensive development of permafrost and substantial reserves of ground ice has exerted critical roles in climate change, ecosystem transition, water resource, carbon budget, and infrastructure of QXP (Zhao et al., 2020; Liu et al., 2022a; 2022b). Accordingly, the QXP has been becoming a hot region for scientists from different research fields (Wang et al., 2006; Yang et al., 2019; Zhao et al., 2021). During recent decades, the QXP has been experiencing severe warming over the past 50 years (Yao et al., 2013; Ran et al., 2022; Kuang and Jiao, 2016), which leads to accelerated permafrost degradation (Wu and Zhang, 2010; Zhao et al., 2021), and thereafter greatly affected the plateau water-eco environment-carbon cycle systems (Wang et al., 2023a; Yi et al., 2014; Liu et al., 2022).

So far, due to the harsh climate conditions, inconvenient transportations, and high experimental costs of site-specific field data, there has been a lack of comprehensive research on different water bodies in permafrost regions over a long time on the QXP, making it challenging to study the water cycle and hydrological processes associated with changing permafrost. In addition, traditional method (e.g., modelling, GRACE satellite technique) is thus difficult to delineate the processes of ice-water transition truly and comprehensively, greatly increasing the uncertainties of evaluation results about the impacts of permafrost degradation on the hydrological processes (Guo et al., 2017). Hydrogen and oxygen stable isotopes ($\delta^{18}O$, δD) are widely existing natural tracers, which are considered to be ideal tools to identify temporal-spatial patterns of precipitation-river-lake-groundwater systems (Knapp et al., 2019; Narancic et al., 2017; Vystavna et al., 2021) and therefore to delineate hydrological connectivity under degrading permafrost (Wang et al., 2022; Streletskiy et al., 2015; Yang et al., 2019). Furthermore, the stable isotopes can well document the signals of ice-water phase transition and freezing history, making them provide convenient means for investigating of ground ice evolution (Michel, 2011; Lacelle et al., 2013; Porter et al., 2019) in permafrost.

Accordingly, continued observations of the stable isotope data, required to understand the changes of hydrological processes and water vapor cycles linked with permafrost degradation and ground ice melt, are therefore of great importance. However, the acquisition of long time series stable isotopic data in permafrost-dominated catchment on the QXP is challenging, especially for thermokarst lakes/ponds and ground ice on the QXP, which are extremely scarce. It greatly limits the deep understanding of the hydrological processes under thawing permafrost.

In this paper, we provide information on the study site and full documentation of the water components in a typical permafrost watershed (Beiluhe Basin, BLH) on the QXP. The data sets presented here, including the stable isotopes of daily precipitation, monthly isotope data of surface waters (stream and thermokarst lakes/ponds) and groundwater, and ground ice within 20 m in depth, will be of great value for tracking water vapor cycles, for capturing the signals of permafrost thawing and delineating the hydrological routines of permafrost meltwater, and in continuing baseline studies for future permafrost degradation trend analysis and water resources evaluations on the QXP. Special emphasis is given to the critical role of BLH for research in the hinterland of QXP to diagnose the effect of thawing permafrost.

2 Study area

A typical permafrost catchment, namely the Beiluhe Basin (BLH), was selected to comprehensively observe the hydrological processes under changing permafrost. The BLH is situated in the interior of the QXP, with elevations of 4,500 to 4,600 m.s.l. It is considered as a core region of the Hoh Xil Nature Reserve region and provides the best habitats for wild animals on the QXP. The BLH is also identified as one of the most fragile and sensitive ecosystems in the world due to the diversities in the ecosystems, which including swamp meadow, alpine meadow, degrading alpine

https://doi.org/10.5194/essd-2024-54
Preprint. Discussion started: 21 March 2024

meadow, alpine steppe, desert alpine grassland, sparse grassland (Yin et al., 2017). According to the meteorological station of BLH, between 2017 to 2022, the annual mean air temperature ranged between -3.57 °C (2019) and -2.43 °C (2022), the annual precipitation ranged between 393.71mm (2020) and 555.99 mm (2018), the duration of negative air temperature exceeds 200 d.

The BLH is closely connected with the Source Area of Yangtze River (i.e., the Tuotuohe River), and is characterized by a complex hydrological system of streams (Yang et al., 2017), thermokarst lakes (Yang et al., 2016; Lin et al., 2010, Niu et al., 2011), groundwater (springs), as well as abundant ground ice (Yang et al., 2013; 2016). Thermokarst lakes are widely distributed in the basin, with a total lake-number of more than 1200 (Luo et al., 2015) which are showing gradual increase trend. In addition, controlled by the piedmont faults of Gushan Mountain (Fig. 1) in the BLH, the natural springs are extensively exposed on the ground, which are the main sources of small streams. The connectivity of lakes, streams, groundwater, as well as melting water from permafrost and ground ice exerted important roles on how ecological and hydrological systems are propagated in this basin.

The BLH is located in the zone of continuous ice-rich permafrost in the Changtang Basin. The permafrost thickness is approximately 20–80 m thick. Mean annual ground temperature (MAGT) at 15 m depth ranges from -1.8 to -0.5°C and the active-layer thickness is 1.6–3.4 m (Wu et al., 2015). Ground ice is abundant in this region, and as high as 70% of this area has a volumetric ice content (VIC) higher than 30% (Luo et al., 2015). Most of the ground ice in the BLH is identified as excess ice (Niu et al., 2002), which could melt out to recharge supra-permafrost water (springs) or even surface water (Yang et al., 2016). Accordingly, the BLH is a natural laboratory to conduct field hydrological observations, the observation data can facilitate the developments of human infrastructure and ecological restoration of QXP.

https://doi.org/10.5194/essd-2024-54
Preprint. Discussion started: 21 March 2024

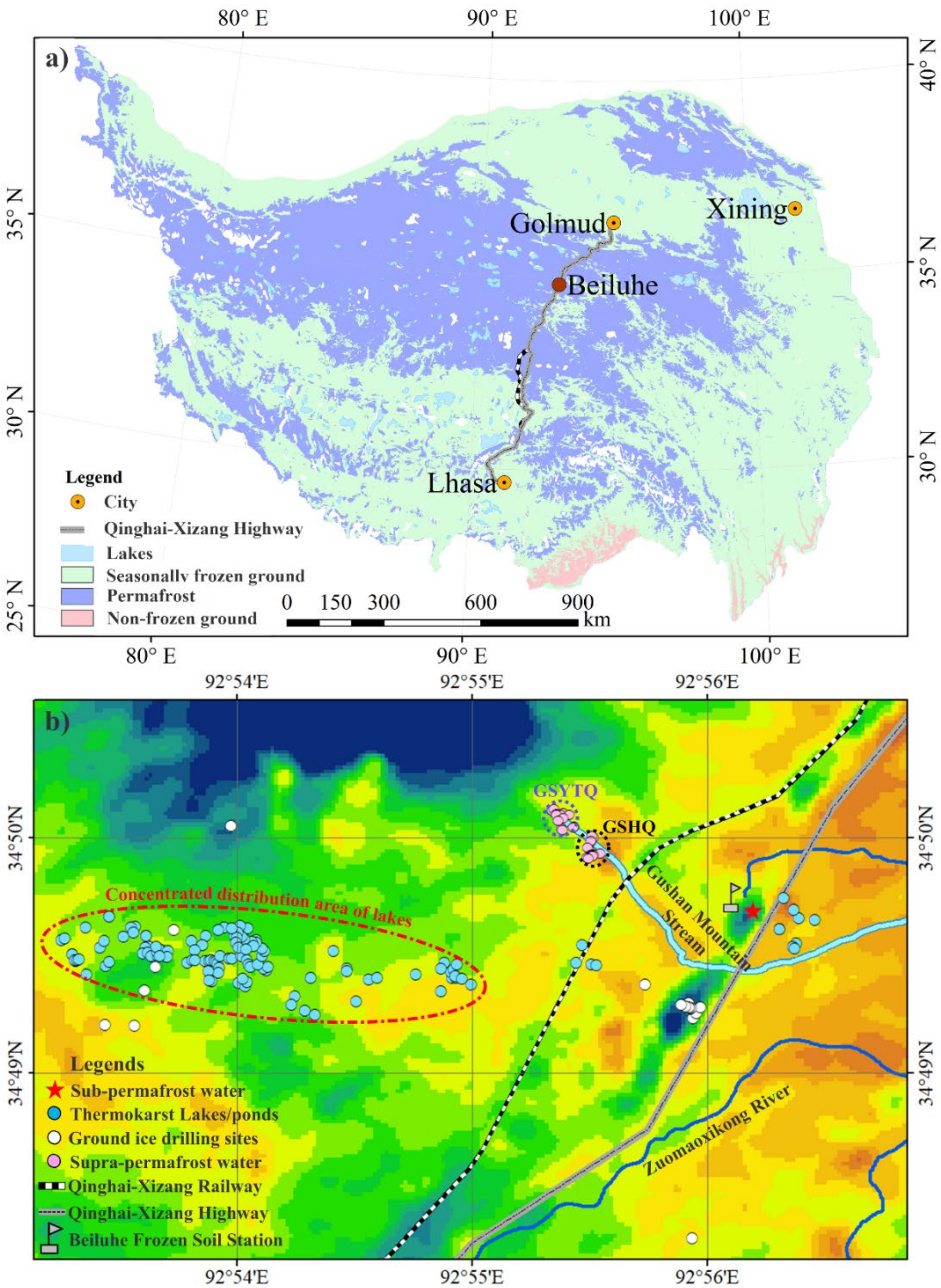

Figure 1: Location of study area on the QXP (a) and specific sampling sites of different water components (b) in the BLH.

https://doi.org/10.5194/essd-2024-54
Preprint. Discussion started: 21 March 2024

3 General design of the monitoring network

From 2017 to 2022, we set up sampling sites of precipitation, stream, thermokarst lake/pond, groundwater (including supra-permafrost water and sub-permafrost water), and ground ice in the BLH basin (Fig. 1). The precipitation stable isotope sampling site was setup at the BLH frozen soil station (Fig. 1). A rain gauge and a steel plate were installed to collected daily rain and snow samples, respectively. In addition, we select a typical small stream (defined as Gushan Mountain Stream, GMS) in the BLH Basin, which originates from four natural springs in foothill of the Gushan Mountain (Fig. 2; Fig. S1). This stream is 4.8 km in length. The vegetation along this stream is mainly composed of deserted steppe. A total of 25 fixed points along the stream were selected to collect water samples during the ice-free seasons between June and October. Furthermore, a typical thermokarst lake belt located in the southwestern of the BLH station on the QXP were selected to observe lake water balance (Fig. 1). For the groundwater observation, we selected two types of natural springs (Fig.1; 2) and identified them as supra-permafrost water, which including several opening springs along the both sides of the observation stream (named as GSHQ) and several opening springs in the source area of this stream (named as GSYTQ) (Fig. 1). In addition, one drinking spring (CSQ) was identified as the observation site of sub-permafrost water behind the BLH station (Fig. 1). In order to detect the permafrost changes and clarify the characteristics of ground ice conditions, 17 boreholes (20 m in depth) were drilled in the BLH basin (Fig. 1). All visible ice samples were collected in the field.

Meanwhile, an auto meteorological station is set up in the center of the BLH since 2005. Air temperature is measured in a solar radiation shield at 2.0 m above the ground surface. The precipitation amount from nearby meteorological station was measured using a T200B rain/snow gauge (Geonor, Norway), and data were recorded every 30 min. The meteorological data have high quality and continuity with very limited missing data due to regular maintenance by Beiluhe Frozen soil station.

https://doi.org/10.5194/essd-2024-54
Preprint. Discussion started: 21 March 2024

Table 1 Location information on the sampling sites in the Beiluhe Basin

Sampling sites	Precipitation	Stream	Thermokarst lakes/ponds	Springs	Ground ice
Latitude/°	N 34.83	N 34.82~34.84	N 34.82~34.83	N 34.83~34.84	N 34.82~34.83
Longitude/°	E 92.94	E 92.92~92.93	E 92.89~92.93	E 92.92~92.93	E 92.93~92.89
Altitude/m	4628	4668~4697	4704~4752	4752~4771	4629~4691

4. Sample collection and processing

4.1 Sampling and preservation

4.1.1 Precipitation sampling work

According to the International Atomic Energy Agency/Global Network of Isotopes in Precipitation (IAEA/GNIP) precipitation sampling guide, a precipitation collector was manually constructed in an open area near the BLH meteorological station. To avoid the contamination of shallow soil, surface water, and windblown snow, this collector was installed 2 m above the ground. We define one complete precipitation day beginning at 20:00 on one day, and ending at 20:00 in the next day, then the one sample was collected. All the rainfall samples were immediately collected after the end of precipitation to minimize the effects of evaporation. Hail and snow samples were filled in pre-cleaned plastic bags and were melted at room temperature (25 °C). A wide mouth stainless steel plate was used to collect as much as samples of light rain and short-time rain/snow events for analysis. Before the sampling, the bottles were washed three times with rain water and then rapidly filled.

Totally, 554 precipitation samples were collected, including 224 rain samples, 203 snow samples, 85 hail samples, and 42 sleet samples.

4.1.2 Stream, thermokarst lakes/ponds, and groundwater sampling

Samples of thermokarst lakes/ponds and streams (Fig. 2) were collected by hand using a self-made water sample collector at monthly intervals during ice-free seasons (between May and October) from 2017 to 2022 in the BLH Basin (Fig. 1). Due to the Covid-19 and lockdown policies in China, only two months' sampling work was conducted. Lake water samples were taken at the centre of lakes from 20–

https://doi.org/10.5194/essd-2024-54
Preprint. Discussion started: 21 March 2024

40 cm below water surface. The running water samples of stream water samples were collected at each fixed point 20-30 cm beneath the water surface. In addition, the supra-permafrost water and sub-permafrost water were randomly collected during each field work.

Totally, as many as 2402 thermokarst lakes/ponds samples, 675 stream water samples (Table 2), 102 supra-permafrost water samples, and 19 sub-permafrost water samples were collected during six years' continuous sampling work.

Figure 2: General conditions of Gushan Mountain Stream (GMS) and distribution of springs (a); Typical feature of one spring gushing outs from sand sediment (b); Overview picture of GMS (c); and Sampling thermokarst lakes in the BLH (d).

https://doi.org/10.5194/essd-2024-54
Preprint. Discussion started: 21 March 2024

191 **Table 2 Sampling descriptions of surface water in the BLH**

Sampling Information		Sampling size	
		Thermokarst lake/pond	Stream
Sampling date	Jun-17	23	25
	Jul-17	76	25
	Aug-17	74	25
	Sep-17	99	25
	Oct-17	72	25
	May-18	74	N.A
	Jun-18	14	25
	Jul-18	45	25
	Aug-18	110	25
	Sep-18	93	25
	Oct-18	106	25
	May-19	80	N.A
	Jun-19	115	25
	Jul-19	134	25
	Aug-19	87	25
	Sep-19	85	25
	Oct-19	110	25
	Jun-20	86	25
	Jul-20	124	25
	Aug-20	116	25
	Sep-20	93	25
	May-21	73	25
	Jun-21	70	25
	Jul-21	100	25
	Aug -21	100	25
	Sep-21	94	25
	Jun-22	75	25
	Jul-22	74	25
Total sample size		2402	675

https://doi.org/10.5194/essd-2024-54
Preprint. Discussion started: 21 March 2024

Open Access Earth System Science Data Discussions

4.1.3 Ground ice sampling

To clarify the characteristics of ground ice and its role on the local hydrological cycles and regional eco-environment, we have designed 17 boreholes (~20 m in depth) in the BLH basin (Fig. 1). A total of 12 boreholes were drilled near the QXH in 2014, and 5 boreholes were distributed in the center of BLH basin, which were drilled between 2011 and 2021. In addition, 2 thaw slumps were dug (Fig. 1). Frozen soil cores were extracted from different depths using a mechanical drilling rig with a drilling diameter of 157 mm (Fig. 3). All visible ground ice samples were collected immediately after the core barrel was pulled out. During sampling work, the disposable PE gloves were used, and the exterior of each sample was removed to avoid contamination from mud and the surplus water in the borehole. Totally, 355 and 4 ground ice samples were collected from 17 boreholes and 2 profiles (Fig. 3; Table 3).

Figure 3: Field permafrost drilling work and various types of ground ice obtained during drilling.

https://doi.org/10.5194/essd-2024-54
Preprint. Discussion started: 21 March 2024

Table 3 Borehole drilling and ground ice sampling information in the BLH

Borehole name	Drilling time	Sampling Depth range /m	Ground ice types	Sample number
BLH-L-1	Aug-2014	4.8-14.9	Pore ice/segregated ice/excess ice	10
BLH-L-2	Aug-2014	2.7-14.3	Pore ice/segregated ice/ excess ice	28
BLH-L-3	Aug-2014	2.9-14.8	Pore ice/segregated ice/ excess ice	20
BLH-L-4	Aug-2014	2.55-14.2	Pore ice/segregated ice/ excess ice	34
BLH-L-5	Aug-2014	2.3-14.0	Pore ice/segregated ice/ excess ice	15
BLH-L-6	Aug-2014	2.6-14.3	Pore ice/segregated ice/ excess ice	11
BLH-R-1	Aug-2014	3.0-12.9	Pore ice/segregated ice/ excess ice	10
BLH-R-2	Aug-2014	1.9-14.9	Pore ice/segregated ice/ excess ice	20
BLH-R-3	Aug-2014	1.25-8.1	Pore ice/segregated ice/ excess ice	17
BLH-R-4	Aug-2014	1.8-11.9	Pore ice/segregated ice/ excess ice	32
BLH-R-5	Aug-2014	1.7-13.8	Pore ice/segregated ice/ excess ice	36
BLH-R-6	Aug-2014	2.1-14.6	Pore ice/segregated ice/ excess ice	22
DZK	Aug-2012	0.0-20.55	Pore ice/segregated ice/ excess ice	27
ZK-1	Aug-2011	12.4-17.4	Pore ice/segregated ice/ Pure ice layer	28
ZK-2	Aug-2011	3.0-7.2	Pore ice/segregated ice/ excess ice	15
ZK-3	Aug-2011	2.6-12.8	Pore ice/segregated ice/ excess ice	13
ZK-4	Aug-2011	2.2-5.5	Pore ice/segregated ice/ excess ice	17
Z	Oct-2021	2.0-3.0	Thaw slump ice	2
FBX	Oct-2021	2.0-3.0	Thaw slump ice	2

https://doi.org/10.5194/essd-2024-54
Preprint. Discussion started: 21 March 2024

4.1.4 Sample storage

Liquid water storage: All the samples were transferred to 100 ml high-density polyethylene (HDPE) bottles. The sample bottles were filled up without bubbles and sealed with parafilm. The collection date sample types (precipitation, lake water, stream water, groundwater) were labeled. For the precipitation samples, the precipitation types (rain, snow, hail) were recorded. All the samples were stored at 4°C and shipped to the State Key Laboratory of Frozen Soil Engineering (SKLFSE) in Northwest Institute of Eco-Environment and Resources, Chinese Academy of Sciences (CAS), China.

Ground ice storage: All the treated raw frozen soil samples were immediately preserved in HDPE bottles. The massive ice and pure ice layers were sealed in the pre-cleaned plastic bags. The depths and drilling site information were recorded. All the frozen soil and ground ice samples were kept frozen at −4°C in the field to avoid sublimation of the ice and evaporation of the water in the soil.

4.2 Sample pretreatment and stable isotope analysis

Before analyzing, each liquid sample was pretreated to remove the impurities through 0.22-μm disposable membrane filters. The frozen soil samples and pure ground ice samples were allowed to completely melt at 4 °C in sealed plastic bags. The supernatant water from thawed soil and meltwater from ground ice were also filtered through a 0.22-μm membrane. The processed liquid water samples were filled in 2 ml analytical vial and were stored in a cold room (4 °C) in the dark for the stable isotopes ($\delta^{18}O$ and δD) analysis within 1 week.

The $\delta^{18}O$ and δD ratios were measured at SKLFSE, using an Isotopic Liquid Water and Water Vapor Analyzer (Picarro L2130-i, U.S.) based on the wavelength-scanned cavity ring down spectroscopy technique. The analyzing accuracy was less than 0.02 ‰ for the $\delta^{18}O$ value measurements and 0.05 ‰ for the δD value measurements (Yang et al., 2023). The isotopic values were reported using notation representing the per mille (‰) relative difference with respect to the IAEA standard Vienna Standard Ocean Water (VSMOW) standard following Eq. (1):

$$\delta=(Rsa/Rst\text{-}VSMOW-1) \times 1000 ‰$$

4.3 Quality control of data

4.3.1 Sampling errors

The precipitation samples were transferred to HDPE bottles immediately. If multiple rain/snow events were occurred during one sampling day, the water sample from one single precipitation event was firstly collected. At the end of one complete sampling day, all the samples collected from single event were mixed. If the precipitation types changed during one sampling day, different samples were collected separately. The final complete samples were kept cool at 4 °C. All we have done is to avoid the influence of evaporation on enrichment of D and ^{18}O and ensure the originality of samples.

During the sampling work of thermokarst lakes/ponds and streams, we do our best to control the sampling time at the same period during every month (On the 29th-30th of each month) to make sure that all the samples can represent the average level of the whole month. The sampling HDPE bottles were precleaned three times using the raw water. Lake water was taken at the center of lakes from 20–40 cm beneath water. The running water samples of stream were collected at each fixed point 20-30 cm beneath the water surface. All these conducted procedures are needed to avoid the impact of evaporation on the original isotope signals of lake and stream water.

4.3.2 Analytic errors

Before we started to analyze the samples, we firstly prepared 14 distilled or tap water samples with the same stable isotopes to test the stability of our analyzer. The precisions of the $\delta^{18}O$ and δD values were calculated by calculating the 1-sigma standard deviation of groups of 12 injections and then calculating the average of these standard deviations. The drift of the analyzer was determined by taking the mean of these same 12 groups of measurements and calculating the difference between the maximum and minimum means. All these measured precision and drift values were less than those of the guaranteed precision (0.025‰ and 0.1‰ for $\delta^{18}O$ and δD) and drift values (0.2‰ and 0.8‰ for $\delta^{18}O$ and δD), indicating that the analyzer achieve both a good repeatability and a good reproducibility. Five laboratory standards for each group of 10 samples were used for instrument calibration: with $\delta^{18}O$ values of −21.28‰, −16.71‰, −11.04‰, −7.81‰, and −2.99‰, and δD values of −165.7‰, −123.8‰, −79.6‰, −49.2‰, −9.9‰.

https://doi.org/10.5194/essd-2024-54
Preprint. Discussion started: 21 March 2024

To avoid memory effects, the first three results of measurements were discarded and arithmetic mean values were calculated from the last three injections. During the analyzing process, the real-time data of water concentration of all injections were controlled within a range between 19000 ppm and 20000 ppm and with a standard deviation of less than 200 ppm. Once the water concentration values appear to decrease, the work was stopped and the syringe was detached to wash using the deionized water. All measurements were post-processed with the Picarro ChemCorrect™ software to monitor the organic contamination and correct the data.

5 General characteristics of stable isotopes in different water components

5.1 Variations in the stable isotopes of different water components

5.1.1 Precipitation

The stable isotopes of precipitation exhibit a remarkable seasonal trend during six years' observations (Fig. 4). The $\delta^{18}O$ and δD of the local precipitation in the BLH Basin ranged from -30.44‰ to 6.20‰ and from -237.99‰ to 65.45‰, respectively. The d-excess ranged between -37.51‰ and 44.52‰. The amount-weighted average values of annual precipitation are -10.94‰, -72.11‰, and 15.41‰ for $\delta^{18}O$, δD, and d-excess, respectively. As shown, the $\delta^{18}O$ and δD display distinct seasonal patterns with high values in summer and low values in winter (Fig. 2; Fig. S2), it is due to the transitions of moisture sources and the influence of local climate conditions (Guo et al., 2022; Tian et al., 2005; Guan et al., 2013; Bershaw et al., 2012).

5.1.2 Surface water bodies

For comparison, the $\delta^{18}O$ and δD of thermokarst lakes/ponds more positive than those of precipitation due to strong evaporation and resultant enrichments of heavier isotopes in lake water (Yang et al., 2016; Narancic et al., 2017; Ala-aho et al., 2018). The $\delta^{18}O$ ranged from -14.39‰ to 5.72‰ (mean: -5.98‰), the δD is between -104.07‰ and 22.59‰ (mean: -47.96‰), and the d-excess is ranged from –35.76‰ to 21.79‰ (mean: -0.14‰), respectively. Similarly, the isotopic patterns of thermokarst lakes/ponds exhibited strong seasonal variations (Fig. 4; Fig. S3), which is due to the transition of source waters and evaporation differences (Narancic et al., 2017; Yang et al., 2021;

Aichner et al., 2022; Zhu et al., 2022). Generally, the isotopic contents of lakes/ponds are lower in August and September (Fig. 4; Fig. S3), which is attributed to the recharges of monsoonal precipitation and isotopic-negative water fed by melting ground ice (Gibson et al., 2015; Yang et al., 2021). In comparison, isotopes of lakes/ponds are positive in May, June, July, and October (Fig. 4; Fig. S3) due to evaporation and isotopic-positive precipitation.

For the streams, the isotope values varied from -13.67‰ to -7.19‰ ($\delta^{18}O$, mean: -11.07‰) and from -83.76‰ to -53.26‰ (δD, mean: -73.56‰), and the d-excess is ranged from -0.59‰ to 25.55‰ (mean: 14.98‰), respectively. The mean values are equivalent to the average levels of precipitation in the BLH. Compared with thermokarst lakes/ponds, the stable isotopes of streams exhibited relatively stable patterns (Fig. 4) due to short residence time (Yang et al., 2021; Wang et al., 2023b; Song et al., 2017). However, the stream isotopes also represented seasonal variations during six year's observation (Fig. 4; Fig. S4), lower values were prevailing in August and September. The temporal changes of stream isotopes are mainly influenced by the seasonal variability of evaporation (Yang et al., 2017) and differences in the source water, i.e., alternative replenishment of precipitation, melting ground ice, and groundwater (Streletskiy et al., 2015; Yang et al., 2019; Ala-aho et al., 2018).

The two kinds of supra-permafrost water (i.e., GSHQ and GSYTQ) exhibited similar seasonal trend (Fig. 4). For comparison, the GSHQ displayed relatively more positive isotopic peaks during whole sampling periods (Fig. 4), with $\delta^{18}O$ ranging from -13.28‰ to -5.76‰ (mean: -11.16‰), the δD is ranging between -86.75‰ and -39.04‰ (mean: -74.17‰), and the d-excess varying from 6.47 to 22.45‰ (mean: 15.13‰), respectively. The isotopes of GSYTQ varied from -13.54‰ to -8.36‰ (mean: -11.36‰), the δD is ranging between -83.18‰ and -50.57‰ (mean: -73.79‰), and the d-excess is varying from 4.57 to 25.12‰ (mean: 16.92‰). The isotopic peaks of the two types of springs lagged behind those of precipitation (Fig. 4), indicating replenishments of precipitation via infiltration. By contrast, the stable isotopes of sub-permafrost water are more negative than those of supra-permafrost water, ranging between -12.68‰ and -11.08‰ (mean: -11.77‰) for $\delta^{18}O$, from -83.75‰ to -77.73‰ (mean: -80.68‰) for δD, and from 10.87‰ to 17.71‰ for d-excess (mean: 13.51‰). In addition, they kept nearly stable over long time series (Fig. 4), suggesting unchanged sources of isotopic-negative water during cold periods and insignificant influence by precipitation.

https://doi.org/10.5194/essd-2024-54
Preprint. Discussion started: 21 March 2024

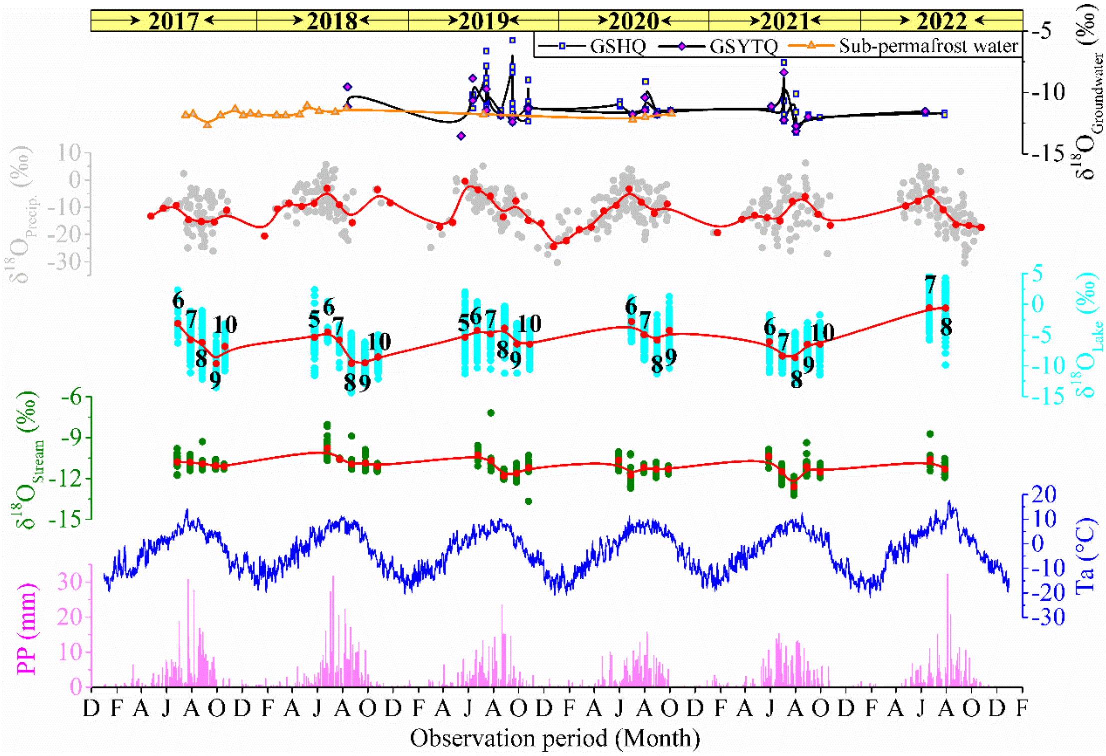

Figure 4: Temporal variations in the δ^{18}O of different water components in the BLH. The numbers denote the observation months of thermokarst lakes/ponds.

5.1.3 Ground ice

The distributions of stable isotope dots of all cores are scattered along depths (Fig. 5). Generally, the δ^{18}O ranging from −15.01‰ to −8.27‰ (mean: -12.19‰), from −113.67‰ to −66.38‰ (mean: -94.44‰) for δD, and between -13.41‰ to 15.50‰ (mean: 3.08‰) for d-excess, respectively. Comparing with the precipitation, majorities of the isotopic points of ground ice are located in the left sides of the mean level of precipitation (Fig. 5), i.e., the ground ice represented more negative isotopes, indicating multi-sources of initial water during ice formation under variable climatic conditions and complex geological contexts on the QXP (Michel, 2011; Yang et al., 2017; 2023; Murton, 2013).

Specifically, the stable isotopes of ground ice varied between different boreholes (Fig. 5; Table 4). It is attributed to the influences of initial source water and complex ice formation mechanism. For instance, the near-surface ground ice is closely related to the recent precipitation and active layer hydrology (Yang et al., 2013; 2017; 2023; Throckmorton et al., 2016), however, the deep-layer ground ice exhibited complicated formation mechanism, including the various source water (meltwater from glacier, permafrost, and snow; lake water; past precipitation; et al) (Yang et al., 2017; Michel et al., 2011; Vasil'chuk et al., 2016; Schwamborn et al., 2014), climate conditions (Yang et al., 2020; Porter et al., 2019), and freeze histories (Yang et al., 2020; Schwamborn et al., 2014; Lacelle et al., 2014). In addition, the isotopic patterns along depths showed marked differences between boreholes (Fig. 4), suggesting influence of lithology on the water migration and freezing fractionation of stable isotopes (Yang et al., 2020; Lacelle, 2014; Fisher et al., 2021). Remarkably, the thaw slump ice represented more negative isotopes than those of drilling ground ice (Fig. 4; Table 4), it is due to the considerable differences in the initial source water and freezing processes. The thaw slump ice is considered to replenished by winter snowmelt water via cracks and freezing quickly (Fritz et al., 2011; Porter et al., 2020). However, the isotopic-positive pore ice in these boreholes is suffered isotope fractionation due to freeze-thaw under climate transitions (Wetterich et al., 2014; Yang et al., 2023).

https://doi.org/10.5194/essd-2024-54
Preprint. Discussion started: 21 March 2024

357 **Table 4 General stable isotope composition of ground ice in the Beiluhe Basin**

Borehole name	Stable isotopes of ground ice								
	$\delta^{18}O$/‰			δD/‰			d-excess/‰		
	Max	Min	Mean	Max	Min	Mean	Max	Min	Mean
BLH-L-1	-11.73	-14.04	-12.97	-91.04	-102.54	-96.80	9.91	2.83	6.99
BLH-L-2	-10.51	-14.46	-13.20	-86.18	-110.16	-101.94	10.62	-2.47	3.69
BLH-L-3	-11.40	-15.01	-12.79	-92.70	-113.67	-100.60	11.36	-7.12	1.74
BLH-L-4	-9.12	-14.61	-12.31	-80.38	-108.16	-95.47	13.92	-13.28	3.04
BLH-L-5	-10.21	-14.10	-12.74	-89.03	-108.60	-100.18	8.08	-7.31	1.74
BLH-L-6	-10.13	-13.33	-11.65	-86.92	-105.42	-96.07	4.42	-10.25	-2.91
BLH-R-1	-9.27	-13.12	-11.90	-80.29	-100.65	-90.81	9.26	-6.14	4.40
BLH-R-2	-10.00	-14.34	-12.53	-80.87	-102.85	-93.51	15.50	-0.91	6.72
BLH-R-3	-11.49	-14.05	-12.80	-90.83	-103.00	-97.52	11.46	-1.65	4.86
BLH-R-4	-11.05	-14.05	-12.68	-94.60	-102.26	-98.47	11.46	-8.48	2.96
BLH-R-5	-9.63	-13.94	-12.41	-84.81	-103.35	-96.29	11.03	-7.77	2.99
BLH-R-6	-8.41	-14.22	-11.84	-75.19	-108.31	-93.11	9.21	-9.18	1.57
DZK	-8.27	-12.29	-10.80	-66.38	-91.83	-85.07	8.02	-2.58	1.31
ZK-1	-10.35	-12.25	-11.80	-83.57	-89.76	-88.13	8.40	-0.79	6.26
ZK-2	-9.66	-13.12	-11.85	-78.77	-102.12	-93.61	7.41	-13.41	1.20
ZK-3	-9.21	-13.16	-11.44	-74.28	-103.61	-90.87	11.83	-13.22	0.66
ZK-4	-9.08	-12.92	-10.93	-69.92	-96.39	-84.38	9.68	-9.12	3.05
TSI	-14.28	-14.68	-14.47	-93.24	-96.30	-94.93	21.18	20.24	20.86

https://doi.org/10.5194/essd-2024-54
Preprint. Discussion started: 21 March 2024

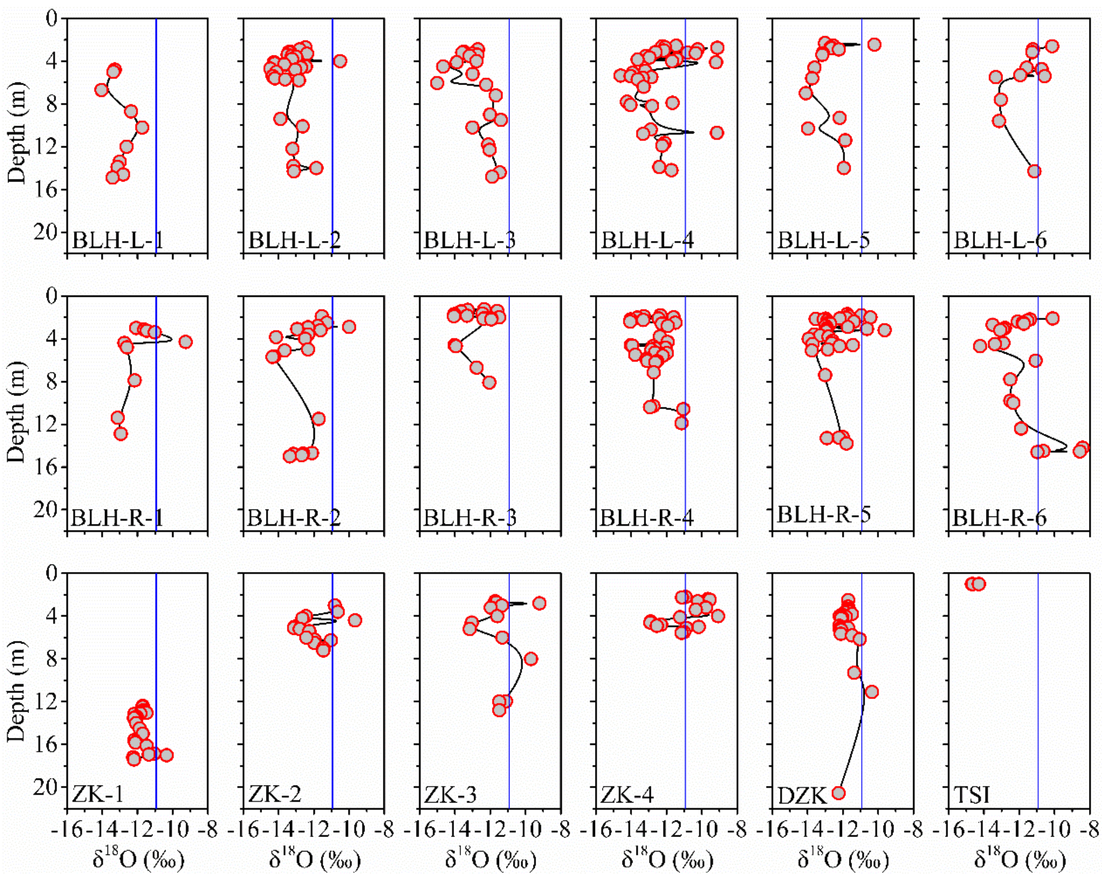

Figure 5: Variations in the stable isotopes of ground ice along depths in the BLH

5.2 $\delta^{18}O$-δD relations and hydrological connections

5.2.1 $\delta^{18}O$-δD relationships of different water components

The local meteoric water line (LMWL), determined by ordinary least square regression using the daily isotopic data during six years (2017-2022), is expressed as: $\delta D=7.97\delta^{18}O+15.26$ ($r^2=0.96$). The slope is nearly identical to that of the global meteoric water line (GMWL; Craig, 1961). However, the intercept is much higher (Fig. 6) due to the influences of continental recycled moisture and westerlies on the QXP (Tian et al., 2005; Yao et al., 2013).

The $\delta^{18}O$–δD diagrams of lakes, streams, and groundwater were built using the monthly stable isotopic values, and defined as local evaporation line (LELs). The LELs observed during six years are

https://doi.org/10.5194/essd-2024-54
Preprint. Discussion started: 21 March 2024

calculated as: $\delta D=5.88\delta^{18}O-12.80$ ($r^2=0.95$), $\delta D=4.89\delta^{18}O-19.41$ ($r^2=0.83$), $\delta D=5.69\delta^{18}O-10.50$ ($r^2=0.85$) (supra-permafrost water), and $\delta D=3.54\delta^{18}O-39.06$ ($r^2=0.92$) (sub-permafrost water), respectively. The slopes of the three LELs are all lower than those of LMWL (Fig. 6), and ranging between 4 and 6, indicating strong evaporation (Cui et al., 2017; Yang et al., 2019). Interestingly, the correlation coefficients of streams and supra-permafrost water are much lower (less than 0.9) and the slopes are smaller than those of precipitation and lakes/ponds (Fig. 6), which may be affected by the transitions of source water during warm seasons and the evaporative concentration of isotopes.

The $\delta^{18}O$–δD relationship for ground ice was established using the stable isotopic values of the ice samples, and the correlation is defined as the freezing line (Souchez et al., 2000). In this study, the freezing line of the ground ice at 16 borehole sites were calculated as: $\delta D=5.36\delta^{18}O-29.15$ ($r^2=0.73$), which is significantly different from the LMWL (Fig. 6). The difference reflects the freezing characteristics of liquid water under different conditions (Lacelle, 2011). Our freezing slope in between 6.2 and 7.3 were usually obtained during equilibrium freezing Rayleigh-type fractionation (Lacelle, 2011). The lower correlation coefficient (Fig. 6) suggests variable freezing rates (Souchez et al., 2000), kinetic isotopic fractionation during ice formation (Souchez et al., 2000), as well as the influence of the initial source water of the ground ice at different sites (Lacelle, 2011; Yang et al., 2017a).

https://doi.org/10.5194/essd-2024-54
Preprint. Discussion started: 21 March 2024

Open Access Earth System Science Data Discussions

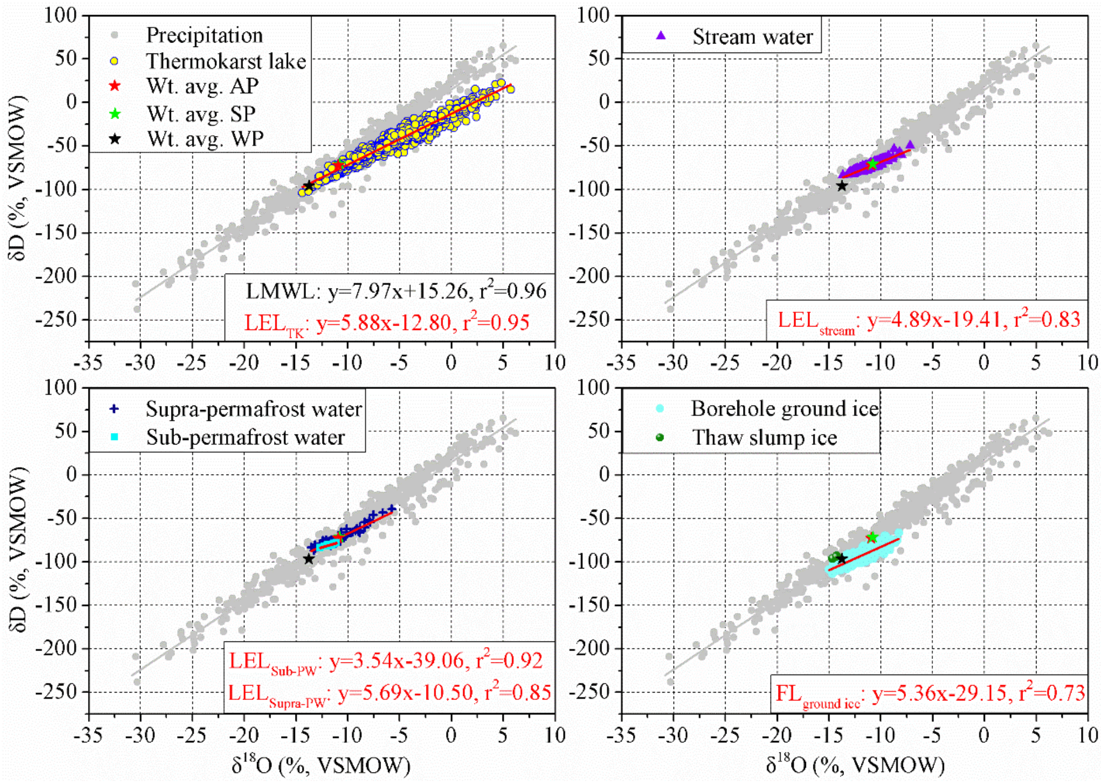

Figure 6: The relation between δD and δ^{18}O of different water components in the BLH.

5.2.2 Hydrological connections between various water components

All the stable isotopes of stream lie on the LMWL (Fig. 6) and embrace in the range of supra-permafrost water (Fig. 7), in addition, the mean value is close to the amount-weighted average value of annual/summer precipitation, indicating the direct recharge of precipitation and supra-permafrost waters. The LEL of thermokarst lakes/ponds significantly deviated from LMWL (Fig. 6 ;7), partial of the isotopic dots overlapped with precipitation, groundwater, and ground ice, indicating the hydrological connections between them (Yang et al., 2016; 2017).

The cluster of ground ice is partly overlapped with precipitation, groundwater, lakes, and stream (Fig. 7). Some of the isotope dots are more positive than the It is indicative of mutual replenishment relations between them. However, the d-excess values of ground ice are more negative than those of river water and more positive than the amount-weighted average value of annual/summer precipitation

https://doi.org/10.5194/essd-2024-54
Preprint. Discussion started: 21 March 2024

(Fig. 7), suggesting the important recharge of active layer water (subjected to evaporation) to the near-surface ground ice (Yang et al., 2013; Throckmorton et al., 2016). In addition, the thaw slump ice exhibited more negative isotopes, which is even lower than the amount-weighted average value of winter precipitation (Fig. 7), indicating the main recharge of snowmelt water (Yang et al., 2020; Opel et al., 2018).

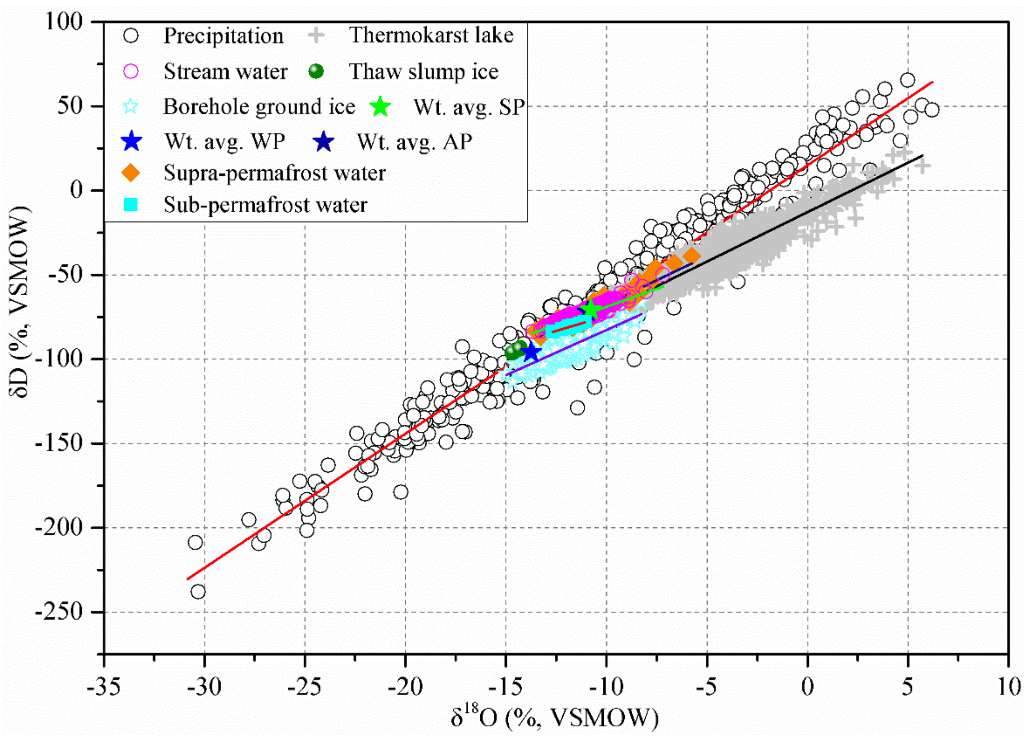

Figure 7: Hydrological connections between different water components.

6 Data availability

All the stable isotope data that support the findings of this study The dataset provided in this paper can be obtained at https://doi.org/10.5281/zenodo.10684110 (Yang, 2024). The link will become publicly available until full publication.

https://doi.org/10.5194/essd-2024-54
Preprint. Discussion started: 21 March 2024

7 Conclusions

From 2017 to 2022, we constructed the first stable isotope monitoring network in a typical permafrost-dominated watershed (namely the Beiluhe Basin, BLH) in central Qinghai-Xizang Plateau (QXP). Totally, we obtained 554 precipitation samples, 2402 lakes/ponds samples, 675 stream water samples, 102 supra-permafrost water samples, and 19 sub-permafrost water samples. Importantly, 359 ground ice samples at different depths from 17 boreholes and 2 profiles were collected, which is the first detailed isotopic data of permafrost ice on the QXP. The following findings are drawn:

1) The stable isotopes of precipitation display distinct seasonal patterns with high values in summer and low values in winter. The slope of LMWL is reflected the global mean. However, the much higher intercept is owing to the influences of continental recycled moisture and westerlies.

2) The thermokarst lakes/ponds and streams exhibit remarkable seasonal patterns in stable isotopes, which is due to the transition of source waters and evaporation differences. The lower isotopic contents in August and September are attributed to the recharges of monsoonal precipitation and melting ground ice. Evaporation enrichment and isotopic-positive precipitation recharges greatly influenced the isotopic patterns in May, June, July, and October. The slopes of the three LELs are all lower than those of LMWL, indicating strong evaporation. The supra-permafrost water was recharged by precipitation via infiltration. By contrast, the sub-permafrost water was replenished by unchanged sources of isotopic-negative water during cold periods.

3) The stable isotopes of ground ice varied between different boreholes. It is attributed to the influences of initial source water and complex ice formation mechanism. The near-surface ground ice was closely related to the recent precipitation and active layer hydrology, however, the deep-layer ground ice exhibited complicated formation mechanism. In addition, variability in the isotopic patterns along depths suggested influence of lithology on the water migration and freezing fractionation of stable isotopes. The freezing line of the ground ice is significantly different from the LMWL, reflected the freezing characteristics of liquid water under different conditions.

This first comprehensive data set provides a new basis for studying the isotopic hydrology and exploring the hydrological effects of degrading permafrost on the QXP. It also enriches the cryospheric database of the Northern Hemisphere.

https://doi.org/10.5194/essd-2024-54
Preprint. Discussion started: 21 March 2024

Author contributions

YY and QW conceived the idea of the study. YY designed the isotope observation network and completed the manuscript. XG and ZZ analyzed water samples and plotted figures. LZ, HY, and DZ participated the field work. JC and GL provided and analyzed the meteorological data.

Competing interests

The contact author has declared that none of the authors has any competing interests.

Acknowledgements

This work was supported by the Key Research Program of Frontier Sciences, CAS (Grant No. ZDBS–LY–DQC026), the National Natural Science Foundation of China (Grant No. 41871062; 42177073), and the foundation of the State Key Laboratory of Frozen Soil Engineering (Grant No. SKLFSE–ZT–202118). We give special thanks to Hong Tan, Yandong Hou, Jing Zhan, Siru Gao, Guanli Jiang, and Peng Zhang for their kind help during field sampling work.

https://doi.org/10.5194/essd-2024-54
Preprint. Discussion started: 21 March 2024

References

[1] Aichner, B., Dubbert, D., Kiel, C., Kohnert, K., Ogashawara, I., Jechow, A., ... & Berger, S. A. 2022. Spatial and seasonal patterns of water isotopes in northeastern German lakes. Earth System Science Data, 14(4), 1857-1867.

[2] Ala-aho, P., Soulsby, C., Pokrovsky, O., Kirpotin, S.N., Karlsson, J.P., Serikova, S., Manasypov, R., Lim, A., Krickov, I., Kolesnichenko, L.G., 2018. Permafrost and lakes control river isotope composition across a boreal-arctic transect in the Western Siberia lowlands. Environmental Research Letters, 13(3): 034028.

[3] Bershaw, J.; Penny, S.M.; Garzione, C.N. 2012. Stable isotopes of modern water across the Himalaya and eastern Tibetan Plateau: Implications for estimates of paleoelevation and paleoclimate. J. Geophys. Res. Atmos, 117.

[4] Biskaborn, B.K., Smith, S.L., Noetzli, J., Matthes, H., Vieira, G., Streletskiy, D.A., ... & Lantuit, H., 2019. Permafrost is warming at a global scale. Nature communications, 10(1), 264.

[5] Brown, J., Sidlauskas, F. J., & Delinski, G. F. 1997. Circum-arctic map of permafrost and ground ice conditions.

[6] Cheng, G.D., Jin, H.J. 2013. Permafrost and Groundwater on the Qinghai-Tibet Plateau and in Northeast China. Hydrogeology Journal, 21 (1): 5-23.

[7] Cheng, G., Zhao, L., Li, R., Wu, X., Sheng, Y., Hu, G., Zou, D., Jin, H., Li, X., Wu, Q., 2019. Characteristic, changes and impacts of permafrost on Qinghai-Tibet Plateau. Chinese Science Bulletin, 64(27), 2783-2795.

[8] Connon RF, Quinton WL, Craig JR, Hayashi M. 2014. Changing hydrologic connectivity due to permafrost thaw in the lower Liard River valley, NWT, Canada. Hydrological Processes, 28(14): 4163–4178.

[9] Craig, H. 1961. Isotopic variations in meteoric waters. Science, 133(3465), 1702-1703.

[10] Cui, J., Tian, L., Biggs, T. W., & Wen, R. 2017. Deuterium-excess determination of evaporation to inflow ratios of an alpine lake: Implications for water balance and modeling. Hydrological Processes, 31(5), 1034-1046.

[11] Douglas, T. A., Hiemstra, C. A., Anderson, J. E., Barbato, R. A., Bjella, K. L., Deeb, E. J., ... & Wagner, A. M., 2021. Recent degradation of Interior Alaska permafrost mapped with ground surveys, geophysics, deep drilling, and repeat airborne lidar. The Cryosphere, 15(8), 3555-3575.

[12] Fisher, D.A., Lacelle, D., Pollard, W., Faucher, B., 2021. A model for stable isotopes of residual liquid water and ground ice in permafrost soils using arbitrary water chemistries and soil-specific empirical residual water functions. Permafrost and Periglacial Processes, 32(2): 248-260.

[13] Fritz, M., Wetterich, S., Meyer, H., Schirrmeister, L., Lantuit, H., & Pollard, W. H. 2011. Origin and characteristics of massive ground ice on Herschel Island (western Canadian Arctic) as revealed by stable water isotope and hydrochemical signatures. Permafrost and Periglacial Processes, 22(1), 26-38.

[14] Gibson, J. J., Birks, S. J., Yi, Y., & Vitt, D. 2015. Runoff to boreal lakes linked to land cover, watershed morphology and permafrost thaw: a 9-year isotope mass balance assessment. Hydrological Processes, 29(18), 3848-3861.

[15] Guan, H., Zhang, X., Skrzypek, G., Sun, Z. and Xu, X., 2013. Deuterium excess variations of rainfall events in a coastal

https://doi.org/10.5194/essd-2024-54
Preprint. Discussion started: 21 March 2024

area of South Australia and its relationship with synoptic weather systems and atmospheric moisture sources. Journal of Geophysical Research: Atmospheres, 118(2), 1123–1138.

[16] Guo, D., Wang, H., Wang, A., 2017. Sensitivity of historical simulation of the permafrost to different atmospheric forcing data sets from 1979 to 2009. Journal of Geophysical Research: Atmospheres, 122(22), 12-269.

[17] Guo, X., Feng, Q., Si, J., & Zhang, X. 2022. Considerable influences of recycled moistures and summer monsoons to local precipitation on the northeastern Tibetan Plateau. Journal of Hydrology, 605, 127343.

[18] IPCC, 2019: Climate Change and Land: an IPCC special report on climate change, desertification, land degradation, sustainable land management, food security, and greenhouse gas fluxes in terrestrial ecosystems.

[19] Knapp, J.L., Neal, C., Schlumpf, A., Neal, M., Kirchner, J.W., 2019. New water fractions and transit time distributions at Plynlimon, Wales, estimated from stable water isotopes in precipitation and streamflow. Hydrology and Earth System Sciences, 23(10): 4367-4388.

[20] Kuang, X., & Jiao, J. J. 2016. Review on climate change on the Tibetan Plateau during the last half century. Journal of Geophysical Research: Atmospheres, 121(8), 3979-4007.

[21] Lacelle, D., Fontaine, M., Forest, A. P., & Kokelj, S. 2014. High-resolution stable water isotopes as tracers of thaw unconformities in permafrost: A case study from western Arctic Canada. Chemical Geology, 368, 85-96.

[22] Lacelle, D., Vasil'chuk, Y. K., 2013. Recent progress (2007–2012) in permafrost isotope geochemistry. Permafrost and Periglacial Processes, 24(2), 138-145.

[23] Lawrence, D. M., Slater, A. G., 2005. A projection of severe near-surface permafrost degradation during the 21st century. Geophysical Research Letters, 32(24).

[24] Lin, Z., Gao, Z., Fan, X., Niu, F., Luo, J., Yin, G., & Liu, M. 2020. Factors controlling near surface ground-ice characteristics in a region of warm permafrost, Beiluhe Basin, Qinghai-Tibet Plateau. Geoderma, 376, 114540.

[25] Liu, F., Qin, S., Fang, K., Chen, L., Peng, Y., Smith, P., & Yang, Y. (2022a). Divergent changes in particulate and mineral-associated organic carbon upon permafrost thaw. Nature communications, 13(1), 5073.

[26] Liu, L., Zhuang, Q., Zhao, D., Zheng, D., Kou, D., & Yang, Y. (2022b). Permafrost Degradation Diminishes Terrestrial Ecosystem Carbon Sequestration Capacity on the Qinghai-Tibetan Plateau. Global Biogeochemical Cycles, 36(2), e2021GB007068.

[27] Luo, J., Niu, F., Lin, Z., Liu, M., & Yin, G. 2015. Thermokarst lake changes between 1969 and 2010 in the beilu river basin, qinghai–tibet plateau, China. Science Bulletin, 60(5), 556-564.

[28] Michel, F. A., 2011. Isotope characterisation of ground ice in northern Canada. Permafrost and Periglacial Processes, 22(1), 3-12.

[29] Murton, J.B., 2013. Ground Ice and Cryostratigraphy. In: Shroder, J.F. (Ed.), Treatise on Geomorphology. Academic Press, San Diego. 173-201.

[30] Narancic, B., Wolfe, B.B., Pienitz, R., Meyer, H., Lamhonwah, D., 2017. Landscape-gradient assessment of thermokarst lake hydrology using water isotope tracers. Journal of Hydrology, 545: 327-338.

[31] Niu, F., Lin, Z., Liu, H., & Lu, J. (2011). Characteristics of thermokarst lakes and their influence on permafrost in Qinghai–Tibet Plateau. Geomorphology, 132(3-4), 222-233.

[32] Opel, T., Meyer, H., Wetterich, S., Laepple, T., Dereviagin, A., Murton, J., 2018. Ice wedges as archives of winter paleoclimate: A review. Permafrost and Periglacial Processes, 29(3): 199-209.

[33] Porter, T. J., & Opel, T. (2020). Recent advances in paleoclimatological studies of Arctic wedge-and pore-ice stable-water isotope records. Permafrost and Periglacial Processes, 31(3), 429-441.

[34] Porter, T.J., Schoenemann, S.W., Davies, L.J., Steig, E.J., Bandara, S., Froese, D.G., 2019. Recent summer warming in northwestern Canada exceeds the Holocene thermal maximum. Nature communications, 10(1): 1631.

[35] Quinton WL, Baltzer LJ. 2013. The active-layer hydrology of a peat plateau with thawing permafrost (scotty creek, canada). Hydrogeology Journal, 21 (1): 201-220.

[36] Ran, Y., Li, X., Cheng, G., Che, J., Aalto, J., Karjalainen, O., ... & Chang, X. 2022. New high-resolution estimates of the permafrost thermal state and hydrothermal conditions over the Northern Hemisphere. Earth System Science Data Discussions, 14 (2), 865–884.

[37] Rogger M, Chirico G, Hausmann H, Krainer K, Brückl E, Stadler P, Blöschl G. 2017. Impact of mountain permafrost on flow path and runoff response in a high alpine catchment. Water Resources Research, 53(2):1288-1308.

[38] Schwamborn G, Meyer H, chirrmeister L, G, F., 2014. Past freeze and thaw cycling in the margin of the El'gygytgyn Crater deduced from a 141m long permafrost record. Climate of the Past, 10: 1109-1123.

[39] Song, C., Wang, G., Liu, G., Mao, T., Sun, X., & Chen, X. (2017). Stable isotope variations of precipitation and streamflow reveal the young water fraction of a permafrost watershed. Hydrological Processes, 31(4), 935-947.

[40] Souchez, R., Jouzel, J., Lorrain, R., Sleewaegen, S., Stiévenard, M., & Verbeke, V. 2000. A kinetic isotope effect during ice formation by water freezing. Geophysical Research Letters, 27(13), 1923-1926.

[41] Streletskiy, D.A., Tananaev, N.I., Opel, T., Shiklomanov, N.I., Nyland, K.E., Streletskaya, I.D., Shiklomanov, A.I., 2015. Permafrost hydrology in changing climatic conditions: seasonal variability of stable isotope composition in rivers in discontinuous permafrost. Environmental Research Letters, 10(9): 095003.

[42] Throckmorton, H.M., Newman, B.D., Heikoop, J.M., Perkins, G.B., Feng, X., Graham, D.E., O'Malley, D., Vesselinov, V.V., Young, J., Wullschleger, S.D., 2016. Active layer hydrology in an Arctic tundra ecosystem: quantifying water sources and cycling using water stable isotopes. Hydrological Processes.

[43] Tian, L., Yao, T., White, J.W.C., Yu, W., Wang, N., 2005. Westerlies moisture transport to the middle of Himalayas revealed from the high deuterium excess. Chinese Science Bulletin, 50(10), 1026–1030.

[44] Vasil'chuk, Y.K., Lawson, D.E., Yoshikawa, K., Budantseva, N.A., Chizhova, J.N., Podborny, Y.Y., Vasil'chuk, A.C., 2016. Stable isotopes in the closed-system Weather Pingo, Alaska and Pestsovoye Pingo, northwestern Siberia. Cold Regions Science and Technology, 128: 13-21.

[45] Vystavna, Y., Harjung, A., Monteiro, L. R., Matiatos, I., & Wassenaar, L. I. (2021). Stable isotopes in global lakes integrate catchment and climatic controls on evaporation. Nature Communications, 12(1), 7224.

[46] Wang, G., Li, Y., Wu, Q., & Wang, Y. (2006). Impacts of permafrost changes on alpine ecosystem in Qinghai-Tibet Plateau. Science in China Series D: Earth Sciences, 49, 1156-1169.
[47] Wang, S., He, X., Kang, S., Fu, H., & Hong, X. (2022). Estimation of stream water components and residence time in a permafrost catchment in the central Tibetan Plateau using long-term water stable isotopic data. The Cryosphere, 16(12), 5023-5040.
[48] Wang, S., He, X., Kang, S., Hong, X., Fu, H., Xue, Y., ... & Guo, H. 2023b. Assessment of streamwater age using water stable isotopes in a headwater catchment of the central Tibetan Plateau. Journal of Hydrology, 618, 129175.
[49] Wang, T., Yang, D., Yang, Y., Zheng, G., Jin, H., Li, X., ... & Cheng, G. 2023a. Unsustainable water supply from thawing permafrost on the Tibetan Plateau in a changing climate. Science bulletin, S2095-9273.
[50] Wetterich, S., Tumskoy, V., Rudaya, N., Andreev, A. A., Opel, T., Meyer, H., ... & Hüls, M. (2014). Ice Complex formation in arctic East Siberia during the MIS3 Interstadial. Quaternary Science Reviews, 84, 39-55.
[51] Wu, Q., & Zhang, T. 2010. Changes in active layer thickness over the Qinghai-Tibetan Plateau from 1995 to 2007. Journal of Geophysical Research: Atmospheres, 115(D9).
[52] Yang, K., Ye, B., Zhou, D., Wu, B., Foken, T., Qin, J., & Zhou, Z. 2011. Response of hydrological cycle to recent climate changes in the Tibetan Plateau. Climatic change, 109, 517-534.
[53] Yang, Y., Guo, X., Wu, Q., Jin, H., & Liu, F. 2023. Formation processes of shallow ground ice in permafrost in the Northeastern Qinghai-Tibet Plateau: A stable isotope perspective. Science of The Total Environment, 863, 160967.
[54] Yang, Y., Wu, Q., Jiang, G., Zhang, P., 2017. Stable Isotopic Stratification and Growth Patterns of Ground Ice in Permafrost on the Qinghai-Tibet Plateau, China. Permafrost and Periglacial Processes, 28(1), 119-129.
[55] Yang, Y., Wu, Q., Jiang, G., Zhang, P., 2020. Ground ice at depths in the Tianshuihai Lake basin on the western Qinghai-Tibet Plateau: An indication of permafrost evolution. Science of the Total Environment,729, 138966.
[56] Yang, Y., Wu, Q., Jin, H., Wang, Q., Huang, Y., Luo, D., Gao, S., Jin, X., 2019. Delineating the hydrological processes and hydraulic connectivities under permafrost degradation on Northeastern Qinghai-Tibet Plateau, China. Journal of hydrology, 569, 359-372.
[57] Yang, Y., Wu, Q., Liu, F., & Jin, H. 2021. Spatial-temporal trends of hydrological transitions in thermokarst lakes on Northeast Qinghai-Tibet Plateau based on stable isotopes. Journal of Hydrology, 597, 126314.
[58] Yang, Y., Wu, Q., Yun, H., 2013. Stable isotope variations in the ground ice of Beiluhe Basin on the Qinghai-Tibet Plateau. Quaternary International, 313, 85-91.
[59] Yang, Y., Wu, Q., Yun, H., Jin, H., Zhang, Z., 2016. Evaluation of the hydrological contributions of permafrost to the thermokarst lakes on the Qinghai–Tibet Plateau using stable isotopes. Global and planetary change, 140, 1-8.
[60] Yang, Y. 2024. Stable isotope dataset of different water components in a tyical permafrost-dominated Basin on the Qinghai–Tibet Plateau [Data set]. Zenodo. https://doi.org/10.5281/zenodo.10684110.
[61] Yao, T., Masson-Delmotte, V., Gao, J., Yu, W., Yang, X., Risi, C., Sturm, C., Zhao, H., He, Y. and Ren, W., 2013. A review of climatic controls on $\delta^{18}O$ in precipitation over the Tibetan Plateau: Observations and simulations. Reviews of

Geophysics, 51(4), 525–548.

[62] Yao, T., Qin, D., Shen, Y., Zhao, L., Wang, N., Lu, A., 2013. Cryospheric changes and their impacts on regional water cycle and ecological conditions in the Qinghai-Tibetan Plateau. Chin. J. Nat, 35(3), 179-186.

[63] Yi, S., Wang, X., Qin, Y., Xiang, B., & Ding, Y. 2014. Responses of alpine grassland on Qinghai–Tibetan plateau to climate warming and permafrost degradation: a modeling perspective. Environmental Research Letters, 9(7), 074014.

[64] Yin, G., Niu, F., Lin, Z., Luo, J., & Liu, M. 2017. Effects of local factors and climate on permafrost conditions and distribution in Beiluhe basin, Qinghai-Tibet Plateau, China. Science of the Total Environment, 581, 472-485.

[65] Zhang X, He J, Zhang J, Polyakov I, Gerdes R, Inoue J, Wu P. 2013. Enhanced poleward moisture transport and amplified northern high-latitude wetting trend. Nature Climate Change, 3: 47-51.

[66] Zhang, T., Frauenfeld, O.W., Serreze, M.C., Etringer, A., Oelke, C., McCreight, J., Barry, R.G., Gilichinsky, D., Yang, D., Ye, H., Ling, F., Chudinova, S., 2005. Spatial and temporal variability in active layer thickness over the Russian Arctic drainage basin. Journal of Geophysical Research: Atmospheres, 110(D16), 1-14.

[67] Zhao, L., Zou, D., Hu, G., Du, E., Pang, Q., Xiao, Y., Li, R., Sheng, Y., Wu, X., Sun, Z., Wang, L., Wang, C., Ma, L., Zhou, H., Liu, S., 2020. Changing climate and the permafrost environment on the Qinghai–Tibet (Xizang) plateau. Permafrost and periglacial processes, 31(3), 396-405.

[68] Zhao, L., Zou, D., Hu, G., Wu, T., Du, E., Liu, G., ... & Cheng, G. 2021. A synthesis dataset of permafrost thermal state for the Qinghai–Tibet (Xizang) Plateau, China. Earth System Science Data, 13(8), 4207-4218.

[69] Zhu, G., Liu, Y., Shi, P., Jia, W., Zhou, J., Liu, Y., ... & Zhao, K. 2022. Stable water isotope monitoring network of different water bodies in Shiyang River basin, a typical arid river in China. Earth System Science Data, 14(8), 3773-3789.